Electrocatalysis by crown-type polyoxometalates multi-substituted by transition metal ions; Comparative study

Rashda Naseer,[a] Sib Sankar Mal,[b,x] Ulrich Kortz,[b] Gordon Armstrong,[c] Fathima Laffir,[c] Calum Dickinson,[c] Mikhail Vagin*,[d] Timothy McCormac[a]

[a]Electrochemistry Research Group, Department of Applied Science, Dundalk Institute of Technology, Dublin Road Dundalk, County Louth, Ireland

[b]Jacobs University, Department of Life Sciences and Chemistry, P.O. Box 750561, 28725 Bremen, Germany

[c]Materials and Surface Science Institute, University of Limerick, Limerick, Ireland

[d]Department of Physics, Chemistry and Biology, Linköping University, SE-581 83, Linköping, Sweden; tel.: +46702753087; mikva@ifm.liu.se

[x]Current address: Department of Chemistry, Science Block, NITK Surathkal, Mangalore-575025, India

Abstract

The difference in electrochemical properties of three crown-type polyoxometalates multi-substituted by Fe^{3+}, Ni^{2+} or Co^{2+} ions and their precursor has been rationalized with respect to their electrocatalytic performances studied in solution and in the immobilized state within the layer-by-layer film formed with a positively charged pentaerythritol-based Ru(II)-metallodendrimer. The film assembly was monitored with electrochemical methods and characterized by surface analysis techniques. An influence of the terminal layer on the electrode reaction and on film porosity has been observed. The electrocatalytic performance of the compounds on nitrite reduction was assessed in solution and in the immobilized state.

Keywords: polyoxometalate, electrocatalysis, layer-by-layer, transition metal ion-substituted crown-type polyoxometalate, nitrite reduction

*Corresponding author

1. Introduction

The electroreduction of nitrite at most electrode surfaces requires a large overpotential, but it has been previously shown to be catalyzed by metallated porphyrins [1-4]. Being catalytic analogues to porphyrins, monosubstituted polyoxometalates (POMs) have the additional advantage of thermal stability, robustness and inertness towards oxidizing environments. Since the late 1980s [5, 6] the electrocatalytic reduction of nitrite has been employed as a classical test for the investigation into the electrocatalytic properties of POMs. The last decade has marked increasing interest in higher nuclearity POM-based transition metal clusters. While such clusters can be obtained from mononuclear precursors [7], the most common approach relies on the use of preformed, highly vacant POMs. Being attractive, the hexavacant $[H_2P_2W_{12}O_{48}]^{12-}$ [8], is however unstable and transforms easily in the presence of transition metal ions [9, 10]. Contrary to this, it's cyclic tetramer $[H_7P_8W_{48}O_{184}]^{33-}$ (P_8W_{48}) [11], is stable over a broad pH range and is now known to display a rich host–guest chemistry. Indeed, it can accommodate transition metals or lanthanide ions [12-17] and reveals electrocatalytic activity towards the reduction of nitrite [18] and hydrogen peroxide [19]. Also, Fe^{3+}- [20], Co^{2+}- and Ni^{2+}-substituted [21, 22] P_8W_{48} anions revealed independent metal ion centres available for redox switching. Introduction of different transition metal ions into POMs enhanced their electrocatalytic performance [21, 23].

The present work focuses on the comparative study of the effect of POM substitution with multiple metal ion centres on catalytic capabilities. This was acquired by the electrochemical characterization of crown-type POM modulated by the multi-substitution with the transition metal ions. Electrocatalytic capabilities of developed compounds to nitrite reduction were assessed in the solution and attached to the electrode. The layer-by-layer (LBL) assembly was utilized as a strategy for the immobilization within the films characterized by the electrochemical and physical methods.

2. Experimental

2.1 Materials

Three crown-type polyoxometalate salts substituted by Fe^{3+} ions ($Li_4K_{16}[P_8W_{48}O_{184}Fe_{16}(OH)_{28}(H_2O)_4]$*$66H_2O$*2KCl) ($Fe_{16}$POM), or Ni^{2+} ions

($K_{14}Li_8Ni_3[Ni_4(H_2O)_{16}(P_8W_{48}O_{184})(WO_2(H_2O)_2]*44H_2O$) ($Ni_7$POM), or Co^{2+} ions ($K_{12}Li_{16}Co_2[Co_4(H_2O)_{16}P_8W_{48}O_{184}]*60H_2O$) ($Co_6$POM) and their precursor salt ($K_{28}Li_5[H_7P_8W_{48}O_{184}]*92H_2O$), were synthesised and characterized according to the literature [22, 24]. The pentaerythritol-based Ru-metallodendrimer [RuD]$(PF_6)_8$ (RuD) was synthesized by M. Zynek *et al.* following the method reported by Constable and Housecroft [25]. Poly(diallyldimethylammonium chloride) (PDDA, MW 20,000) and all other chemicals were purchased from Aldrich and were used without further treatment. HPLC grade water was used for preparation of all aqueous solutions. The aqueous buffer solutions were prepared from 0.5M Li_2SO_4 + 0.5M H_2SO_4 (pH 2.0), 0.5M H_2SO_4 (pH 0.0 - 0.5), 1M LiCl + 1M HCl (pH 1.0 - 3.0), and 1M CH_3COOLi + 1M CH_3COOH (pH 3.5 - 7.0). For the electrocatalysis experiments solutions of $NaNO_2$ and H_2O_2 were freshly prepared before use.

2.2. Apparatus and procedures

2.2.1 Electrochemical measurements

All electrochemical experiments were performed with CHI660 electrochemical work station in a conventional three-electrode electrochemical cell. A glassy carbon electrode (GCE, 3 mm ∅, surface area 0.0707 cm^2) was used as the working electrode, a platinum wire as the auxiliary electrode, and a silver/silver chloride as the reference electrode (3M KCl) in aqueous media in all experiments unless otherwise stated. The working electrode was successively polished with 1.0, 0.3 and 0.05 μm alumina powders and sonicated in water for 10 min after each polishing step. Finally, the electrode was washed with ethanol and then dried with a high purity argon stream immediately before use. Solutions were degassed for at least 20 min with high-purity argon and kept under a blanket of argon during all electrochemical experiments.

The following electrolytes were used: 0.5M Li_2SO_4 (pH 2.0), 1M LiCl (pH 1.0 - 3.0), and 1M CH_3COOLi (pH 3.5 - 7.0). The pH adjustment was done with 0.5M H_2SO_4, 1M HCl and 1M CH_3COOH respectively.

2.2.2 Construction of multilayer assemblies

A clean glassy carbon electrode (GCE) was immersed in the 8% (v/v) PDDA solution for one hour for initial surface modification. Then electrode was then rinsed thoroughly with deionised water and dipped in a 0.25mM solution of the desired POM in pH 2.0 buffer solution for 20 minutes to allow the anionic layer to adsorb (Step 1).

The POM modified electrode was rinsed again thoroughly with deionised water and dried with a high purity nitrogen stream. Then the PDDA-POM-modified electrode was then dipped in a 0.2 mM solution of RuD in acetonitrile for 20 minutes to build up the cationic layer (Step 2). The electrode was then washed with acetonitrile and dried with nitrogen. To build the desired number of layers, steps 1 and 2 were repeated as appropriate.

2.2.3 Electrochemical Impedance Spectroscopy (EIS)

Electrochemical impedance spectroscopy has been carried out in a 10 mM potassium ferricyanide and 10 mM potassium ferrocyanide solution in 0.1 M KCl at a potential of +230 mV (versus Ag/AgCl) from 0.1 to 10^5 Hz with a voltage amplitude of 5 mV. The measurement solution was freshly prepared and constantly degassed with nitrogen during the experiment.

2.2.4 X-ray photoelectron spectroscopy (XPS)

The multilayer films deposited on glass slides covered with indium tin oxide (ITO) were characterised using X–ray photoelectron spectroscopy (XPS). Analysis was performed in a Kratos AXIS 165 spectrometer using monochromatic Al Kα radiation of energy 1486.6 eV. Survey spectra and high resolution spectra were acquired at fixed pass energies of 160 eV and 20 eV respectively. In the near-surface region the atomic concentrations of the chemical elements were evaluated after subtraction of a Shirley type background by considering the corresponding Scofield atomic sensitivity factors. Surface charge was efficiently neutralised by flooding the sample surface with low energy electrons. Core level binding energies were determined using C 1s peak at 284.8 eV as the charge reference.

2.2.5 Scanning electron microscopy (SEM)

LBL films of 12 assembly steps deposited onto ITO slides were characterised by SEM imaging using Hitachi SU-70 field emission scanning electron microscope operating at an accelerating voltage of 3 kV. The low voltage allowed for imaging the multilayer assemblies without the requirement of gold coating.

2.2.6 Atomic force microscopy (AFM)

The LBL films formed on ITO slides were imaged in air using an Agilent 5500 instrument operating in AAC ('tapping') mode, controlled by PicoView 1.10 software. Micromasch NSC14 cantilevers (160 kHz typical resonant frequency, 5 N/m spring constant) were used. All images presented were obtained at 256 pixel resolution. Scan areas and scan speeds were optimized to suit the features observed for each sample; typically, scans of 1 x 1 μm were obtained at a scan speed of 0.7 lines/second. Images were processed using PicoImage Advanced 5.1.1 software. Raw topography and amplitude data images were levelled using a three-point algorithm. Where appropriate, noise was removed by applying a median denoising spatial filter, and line noise arising from artefacts was removed. The resulting topography images are presented as pseudo-colour images. Height parameters were determined for each topography image according to ISO standard 25178.

3. Results and Discussions

3.1 Solution electrochemistry

Figure 1A represents the cyclic voltammogram obtained for the Co_6POM in 0.5 M H_2SO_4 (solid line). Two reversible redox processes with $E_{1/2}$ values of -0.16 V and -0.41 V, which represent the two consecutive eight-electron redox-processes of the POM's tungsten-oxo (W-O) framework (I and II), are observed. Slight splitting of these redox processes into four simultaneous four-electron redox transfers is also apparent in the cyclic voltammogram. The anodic peak at +1.5 V represents the simultaneous one-electron irreversible oxidation of the six cobalt centres ($Co^{2+/3+}$) within POM. The increase of pH to 4.5 (dashed curves) shows a cathodic shifts and subsequent decrease in peak currents for all redox processes, which is an inherent property of POM redox processes [19, 23, 26-29]. The observed pH dependences of the formal potentials for the W-O I and II redox processes points to the involvement of the protons. The cathodic shifts for W-O I redox processes of all compounds of study exceeded 59 mV per unit of pH, which is typical for POM redox processes with the same numbers of both protons and electrons involved [30]. The resulting scan rate study pointed to the diffusion controlled nature of the W-O I and II redox processes. The diffusion coefficients estimated for W-O I redox process of Ni_7POM and Co_6POM by Randles-Sevchik analysis were 0.43 x 10^{-6} cm^2 s^{-1} and 0.35 x 10^{-6} cm^2 s^{-1}, which are one order of magnitude smaller than the diffusion coefficient for POM anion $[S_2Mo_{18}O_{62}]^{6-}$ [31] of significantly smaller molecular weight and charge.

The Fe_{16}POM and Ni_7POM, as well as their precursor, all exhibited solution phase voltammetric behaviour associated with the POM's W-O framework similar to Co_6POM. For the Fe_{16}POM the redox activity associated with the one-electron redox process for the sixteen iron centres appears with an E_{pa} of +0.587 V and an E_{pc} of -0.215 V in pH 2.0. In more alkaline pH the anodic and cathodic waves are shifted cathodically to + 0.280 V and – 0.399 V in pH 4.5, respectively. However, Ni_7POM showed the absence of any Ni^{2+}-associated redox process, which is located out of the anodic limit of available potential window.

The electrochemical reduction of nitrite typically requires a large overpotential at bare electrode surfaces [1]. Due to the inherent instability of HNO_2 (pK_a 3.3) via a disproportionation reaction [28] the electrocatalytic reduction of nitrite has been studied in this contribution at pH 4.5. Figures 1B-1E shows the effect of nitrite upon the redox behaviour of the precursor and Fe_{16}POM, Co_6POM and Ni_7POM where an increase in the cathodic and decrease in the anodic peak currents of the W-O II redox process is clearly observed for all four compounds. This indicates that it is the multiply reduced form of the POM that catalyses the reduction of the added nitrite. Fe_{16}POM and Ni_7POM showed the higher electrocatalytic effects in comparison with Co_6POM and the precursor, which is illustrated by the calibration plots of the voltammetric responses (Fig. 1F). The sensitivity of the responses decreases in the series Fe_{16}POM (330 mA M^{-1} cm^{-2}) ~ Ni_7POM (330 mA M^{-1} cm^{-2}) > Co_6POM (180 mA M^{-1} cm^{-2}) > precursor (100 mA M^{-1} cm^{-2}) with the Fe_{16}POM exhibiting the wider linearity region.

3.2 Metal Substituted P_8W_{48}-RuD LBL films

Figure 2 (A and B) illustrates the voltammetric responses obtained during the construction of an electrode modified with LBL-films composed of the Co_6POM and the RuD cationic moiety. What is apparent is the presence of all the redox processes associated with both the substituted POMs and the RuD moiety. The continuous increase in peak currents due to LBL assembly with both outer layers were more prominent for the W-O II and $Ru^{II/III}$ redox processes, whereas the peak currents associated with the W-O I redox process does not increase markedly with increasing layer number. The decrease of the peak currents for the W-O II and $Ru^{II/III}$ redox couples is observed with any RuD outer layer. (Fig. 2B). The switching effect of the

W-O II framework redox process was up to two times for the oxidation peak and up to three times for the reduction peak at 20 assembly steps. The weaker switching behaviour was observed for the $Ru^{II/III}$ redox process, whereas the currents associated with the W-O I redox process did not change due to LBL assembly.

Figure 2C represents the dependence of measured charges for the $Ru^{II/III}$ redox processes with layer number. The increase of charge illustrates the building the Co_6POM-RuD film. The switching effect of the $Ru^{II/III}$ redox process increases with layer number. Generally, the depositions of substituted POM layers led to a more than two times increase in the $Ru^{II/III}$ redox processes charge. On the contrary, the depositions of RuD layers led to a more than two times decrease of charge. The charges of W-O II redox process reveal the same behaviour with assembly. The possible reason of redox processes switching is an opposite changes in charge interactions between the terminal layer of the assembly and the ions inserting/expelling from/into LBL film for electroneutrality during the Faradaic processes. This oscillatory behaviour is inherent to POM-based LBL films [27]. The surface coverage assessed from the redox peaks charges for even numbers of layers by Faraday's law ($\Gamma = Q/nFA$, where Q – peak charge (C), n – number of transferred electrons, which is equal to 8 for crown type heteropolyanions P_8W_{48} [18], F – Faraday's constant (96485 C mol^{-1}) and A – electrode surface area (0.0707 cm^2)) revealed a continuous growth of redox active material on the electrode surface. W-O II oxidation peak showed up to 2.5 times increase of coverage up to 0.2 nmol cm^2 due to the 15 steps of LBL assembly, whereas $Ru^{II/III}$ oxidation peak gave a 4 times coverage increase up to 2.3 nmol cm^2. Immobilization of Fe_{16}POM by LBL technique led to changes in its voltammetric response. The peak separations for both W-O redox processes were decreased illustrating the increase of electron transfer rate. W-O I redox process was sufficiently suppressed.

Due to the involvement of electrons in the POM redox processes, there is a pH dependency of the POM redox potentials both in solution and in the solid state [19, 23, 28, 29]. The pH dependences of the formal potentials of the W-O I redox process for the substituted POM-RuD films exhibited higher pH shifts than those observed in solution. The involvement of 12 protons for the Ni_7POM-RuD films and 16 protons for the Co_6POM-RuD film have been measured. The W-O II redox process was

characterised by a smaller pH effect. No effect from the nature of the layer's outer layer was observed on the pH dependent nature of the W-O redox processes. $Ru^{II/III}$ redox process does not show any particular shift with the increasing pH illustrating the non-participation of protons in this redox process.

Stability of the film-modified electrodes has been assessed by continuous cyclic voltammetry with 500 cycles at pH 2.0 and pH 7.0 electrolyte solutions. The loss of peak currents of W-O II redox process was not higher than 17% in both tests. Electrode modified with Ni_7POM -RuD LBL film showed no change in peak currents after one month shelf storage.

3.2.1. Kinetics analysis of electrode reactions.

The linear dependences of the peak currents with scan rates from 0.01 V s^{-1} to 2 V s^{-1} have been observed for all redox processes for all POM based LBL films in this contribution. Laviron's theoretical approach for diffusion less electrochemical systems has been applied to the POM-LBL films for the assessment of the kinetics parameters associated with the film's redox processes [32]. The peak separation, ΔE_p, between the anodic and cathodic peaks for the W-O II redox process was higher than the expected 200/n mV, where n = 8 is the number of transferred electrons for the crown type heteropolyanions P_8W_{48} [18]. Thus the transfer coefficient and rate constant for the electron transfer can be determined for the W-O II redox process. A graph of the anodic peak potential as a function of log[scan rate] yielded a straight line with a slope equal to $2.3RT/(1-\alpha)nF$, where n, F, R and T have their usual significance, and α is the transfer coefficient. The heterogeneous rate constants were calculated through the employment of equation 1: [32]

$$\log k = \alpha \log (1 - \alpha) + (1 - \alpha) \log \alpha - \log (RT/nF\nu) - \alpha (1 - \alpha)nF\Delta E_p/2.3RT \ldots..(1)$$

Table 1 represents the kinetic parameters obtained for the W-O II redox process for various POM based LBL modified electrodes. It can be seen that all films exhibit the same transfer coefficient with the heterogeneous rate constants significantly increasing for films based on the Ni_7POM with respect to the Co_6POM-based film. It can be observed also that the higher heterogeneous rate constant obtained for Ni_7POM

is more sensitive for the terminal layer. The peak to peak difference, ΔE_p, for the $Ru^{II/III}$ redox process was lower than 200/n mV, where n = 1. Therefore, the transfer coefficient was equal to 0.5 and the working function of Laviron [32] has been used to determine the ratio between the heterogeneous rate constant and film thickness. The ratio was 20 s^{-1} at 2 V/s, which did not change sufficiently with film composition or the nature of the outer layer in the LBL films. Assuming the film thickness of 10 μm, the value of the heterogeneous electron transfer rate constant for the Ru(III/II) redox processes at a LBL film modified electrode was estimated as 0.02 cm s^{-1}, which is close to the values obtained for the $Ru(III/II)(bpy)_3$ redox process in solution (0.066-0.07 cm s^{-1}) [33].

3.2.3 Electrochemical Impedance Spectroscopy (EIS)

Figure 3A represents Nyquist plot of impedance spectra obtained at an electrode modified with LBL films with different outer layers at a potential of +0.23 V, which is associated with the formal potential for the potassium ferri/ferrocyanide couple. There is a continuous increase in the diameter of observed semicircle, which is associated with an increase in the charge transfer resistance R_{CT} with layer number. The interpretation of the impedance data has been carried out employing the Randles equivalent circuit [27], which consists of a double layer capacitance in series with solution resistance and in parallel with a diffusion branch, i.e. Warburg impedance in series with a charge transfer resistance. The constant phase element was introduced instead of a double layer capacitance, which illustrates non-uniform distribution of capacitance over electrode surface.

It is seen (Fig. 3B), that the increase in R_{CT} with layer number for LBL films of both Co_6POM and Ni_7POM can be described with a single exponential function up to 8 steps of assembly. This effect strongly confirms, that electron transfer between the ferri/ferrocyanide couple and the underlying electrode surface is controlled by coherent electron tunnelling across the LBL film [34], which can be expressed in terms of the tunnelling decay constant β [34, 35]: $R_{CT} = R_{CT}^0 \exp(\beta x)$, where R_{CT}^0 is the factor depending upon both the redox probe and electrode surface properties. The slopes obtained for both POM-based films give almost the same decay constants β approximately of 0.2 per layer. The decay constants for thiol monolayers formed at

gold surfaces per methylene unit are up to two times higher than obtained here [34]. Thus a sufficiently smaller decrease in the electron-tunnelling probability with a length of a spacer is observed here, which probably is evidence of hoping conductivity of the LBL films via the embedded redox sites.

3.2.4 Permeability of LBL films towards different redox probes

The porosity and permeability of the LBL films on electrodes were investigated by voltammetry in presence of the cationic redox probe $[Ru(NH_3)_6]^{3+/2+}$, which is characterised by reversible monoelectronic redox process at -0.24 V (vs Ag/AgCl). The probe can undergo the redox transformation at the underlying electrode surface after diffusion through the multilayer system or within the film by electron transfer mediated by the redox sites within the LBL film [28]. Figure 4 presents the voltammograms obtained for the blank GCE and with electrodes modified with Ni_7POM-RuD LBL films as a function of both layer number and the nature of the outer layer. It can be seen that modifications of the electrode surface with LBL films led to a suppression of the probe's redox peaks indicating the enhanced difficulty of the probe to diffuse through the LBL films for reaction at the underlying electrode. Only electrodes modified with thin LBL film (assembly number 8) and with anionic POM outer layers showed the residual redox activity of the cationic probe at the underlying electrode surface (thick line at Fig. 4A) due to favourable electrostatic interactions between probe and outer layer. The absence of the redox activity at the electrode modified by LBL films with thickness (assembly number 9) with cationic outer layer (Fig. 4B) shows the unfavourable electrostatic repulsion between the probe and outer layer. On the other hand, the increase in the cathodic currents of the W-O I and II redox processes observed in the presence of the probe shows the appearance of an electrocatalytic reduction of oxidized probe due to electron transfer from the POM. The increase in the electrocatalytic currents with increasing film thickness (assembly numbers 16 and 17, Fig. 4C and 4D correspondingly) represents the involvement of redox sites within the film.

3.2.6 Preliminary electrocatalytic properties of LBL films

Nitrite ion reduction has been used previously [6, 36-38] to assess the electrocatalytic activity of LBL films. Figure 5 shows the nitrite concentration dependence of the cathodic current increase of the POM's W-O II redox process observed at an electrode

modified with the Ni_7POM-RuD LBL film of 16 assembly steps. As observed in solution the W-O I redox process is not affected by the presence of NO_2^-, whereas the cathodic peak current for the W-O II process increased greatly (Inset of Fig. 5), accompanying by a decrease in the redox processes anodic peak current. The calibration plot showed two linearity regions, which probably illustrates the complexity of the electrocatalytic process occurring at the LBL film. The sensitivity of nitrite detection estimated at the linearity region of 0.2-0.6 mM was 132 mA M cm^{-2}, which is larger than the reported values of sensitivity obtained at different film-modified electrodes for electrocatalytic reduction of nitrite [39-46]. The significant decrease of sensitivity down to 15.7 mA M cm^{-2} was observed at linearity region of higher nitrite concentrations (0.6-5 mM). In addition, there is no electrocatalytic response between the POM and nitrate up to 10 mM concentration (data not show). The same behaviour was observed with films of all substituted POM and different assembly numbers. Therefore, it might be concluded that the POM multi-substituted with transition metal ions showed excellent selectivity towards the reduction of nitrite. LBL assembly of catalyst led to significant decreases of sensitivity and of linearity regions, which is typical for electrocatalyst surface immobilization.

3.3 Surface analysis of substituted P_8W_{48}-RuD LBL film

3.3.1 X-Ray Photoelectron Spectroscopy (XPS)

Surface composition of the deposited multilayer films on PDDA modified ITO glass slide were determined by performing X-ray photoelectron spectroscopy (XPS) which has a probe depth of approximately 10 nm. The survey spectra (Fig. S1) confirms the presence of the substituted metal ions in their respective multilayer assemblies. The peaks corresponding to the metal ions are more prominent in the high resolution spectra (not shown here) of individual elements. The relative compositions of the elements are quantified in Table S1.

The presence of the Ni_7POM is evident from the Ni 2p doublet peak at binding energy of $2p_{2/3}$ at 855.9 eV, W 4f doublet at 35.2 eV and P 2p at 133.0 eV [47, 48]. High resolution spectrum of C 1s can be decomposed mainly into peaks representitive of C=C (284.8 eV), C-O/C-N (286 eV) and O=C-O/N (288.5 eV). In addition, the related N 1s peak at 400 eV and Ru 3d at 281 eV confirm the presence of pyridine based Ru dendrimer layer. Lithium present in the LBL films could not be identified perhaps due to its concentrations below the detection limit of the instrument (~ < 0.1

atomic %) and its low sensitivity in XPS. Similarly the presence of Co_6POM is evident from the Co 2p peaks at binding energies 781.4 eV respectively.

3.3.2. Atomic force microscopy (AFM)

AFM was conducted at different stages of LBL assembly of films on the ITO to examine the resulting changes in the topography of the multilayers. The dependence of the root mean square height of the surface (S_q), determined during deposition process for both Ni_7POM and Co_6POM, on the assembly number is presented Fig. 6E. Upon depositing the initial PDDA layer on the ITO substrate, the polymer filled in the low-lying valleys on the ITO surface, but followed the contours of the high features on the substrate, resulting in an overall increase in S_q in consistence with the mechanism proposed by Zynek *et al.* [29]. Co^{2+}-substituted POM, The addition of the first POM layer yielded a homogenous surface topography, resulting in a significant reduction in S_q. Following further deposition, globular structures were observed (Fig. 6B and 6C). These globules were of similar shape and distribution for films with POM or RuD terminal layers. However, the associated change in S_q was 5 times smaller for the POM terminal layer than for RuD (3.51 nm vs. 15.9 nm). These observations suggest that the negatively charged POM preferentially fills in the low-lying valleys on the surface, whereas cationic RuD and PDDA layers agglomerate, resulting in increased S_q with respect to the underlying surface. These observations are in agreement with data reported previously [29, 49]. Little phase contrast was seen for all the layers analysed; this suggests that the samples consisted of a homogeneous film within the areas of interest imaged.

3.3.3. Scanning Electron Microscopy (SEM)

The morphologies of multilayer films were also investigated by SEM which showed that the surfaces of all metal ion-substituted POM-RuD films were rather flat with the sizes of the particles on the film being 1-200 nm in diameter (Fig. 6D). No globular structure was observed. Both films were also quite uniform and seemed to be porous.

Conclusions

The molecular engineering via host-guest chemistry allowed the multi-substitution of crown-type POM with a transition metal ions. The introduction of metal ion centres led to the enhancement of electrocatalytic capabilities of designed molecules as it was

shown by the comparative study of electrochemical properties of POMs multi-substituted with Fe^{3+}, Co^{2+} and Ni^{2+} ions in solution and attached to an electrode surface through LBL assembly with a pentaerythritol-based Ru(II)-metallodendrimer. Fe_{16}POM showed the highest electrocatalytic activity for nitrite reduction, which, probably, is due to the largest number of accommodated metal ions. Electrochemical studies of LBL assemblies showed a switching behaviour of the films as well as performance control with the terminal layer and pH.

Table 1. Kinetic parameters of W-O II redox process observed at LBL film-modified electrode.

Type of film	**α**	**k*, cm s^{-1}**
Co_6POM films		
with outer RuD layer	0.76	0.07
with outer POM layer	0.73	0.12
Ni_7POM films		
with outer RuD layer	0.83	4
outer POM layer	0.76	1.1

* estimated at 2 V s^{-1}

References

[1] M.H. Bradley, M.R. Rhodes, T.J. Meyer, Electrocatalytic reduction of nitrite to nitrous oxide and ammonia based on the N-methylated, cationic iron porphyrin complex $[Fe^{III}(H_2O)(TMPyP)]^{5+}$, Inorganic Chemistry, 26 (1987) 1746-1750.

[2] J.N. Younathan, K.S. Wood, T.J. Meyer, Electrocatalytic reduction of nitrite and nitrosyl by iron(III) protoporphyrin IX dimethyl ester immobilized in an electropolymerized film, Inorganic Chememistry, 31 (1992) 3280-3285.

[3] S.H. Cheng, Y.O. Su, Electrocatalysis of Nitric Oxide Reduction by Water-Soluble Cobalt Porphyrin. Spectral and Electrochemical Studies, Inorganic Chemistry, 33 (1994) 5847-5854.

[4] C.H. Yu, Y.O. Su, Electrocatalytic reduction of nitric oxide by water-soluble manganese porphyrins, Journal of Electroanalytical Chemistry, 368 (1994) 323.

[5] B. Keita, L. Nadjo, R. Contant, M. Fournier, G. Herve, Process for the catalytic reduction of nitrogen compounds, and catalysts used, CNRS, France, 1989.

[6] J.E. Toth, F.C. Anson, Electrocatalytic Reduction of Nitrite and Nitric Oxide to Ammonia with Iron-Substituted Polyoxotungstates, Journal of the American Chemical Society, 111 (1989) 2444-2451.

[7] J.-D. Compain, P. Mialane, A. Dolbecq, I.M. Mbomekallé, J. Marrot, F. Sécheresse, E. Rivière, G. Rogez, W. Wernsdorfer, Iron Polyoxometalate Single-Molecule Magnets, Angewandte Chemie-International Edition, 48 (2009) 3077-3085.

[8] R. Contant, J.P. Ciabrini, Preparationon and solution properties of some defect heteropolyanions related to 18-tungsto-2-phosphates (α- and β-isomers), Journal of Chemical Research, Synopsis, 222 (1977) 2601-2617.

[9] A. Ostuni, M.T. Pope, A large heteropolytungstotetracerate(III) based on a new divacant lacunary derivative of the Wells–Dawson tungstophosphate anion, Comptes Rendus de l'Académie des Sciences - Series IIC - Chemistry, 3 (2000) 199-204.

[10] B. Godin, Y. Chen, J. Vaissermann, L. Ruhlmann, M. Verdaguer, P. Gouzerh, Coordination chemistry of the hexavacant tungstophosphate $[H_2P_2W_{12}O_{48}]^{12-}$ with Fe^{III} ions: Towards original structures of increasing size and complexity, Angewandte Chemie-International Edition, 44 (2005) 3072-3075.

[11] R. Contant, A. Teze, A new crown heteropolyanion $K_{28}Li_5H_7P_8W_{48}O_{184}\cdot 92H_2O$: synthesis, structure, and properties, Inorganic Chemistry, 24 (1985) 4610-4614.

[12] S.S. Mal, M.H. Dickman, U. Kortz, A.M. Todea, A. Merca, H. Bögge, T. Glaser, A. Müller, S. Nellutla, N. Kaur, J. van Tol, N.S. Dalal, B. Keita, L. Nadjo, Nucleation process in the cavity of a 48-tungstophosphate wheel resulting in a 16-metal-centre iron oxide nanocluster, Chemistry-a European Journal, 14 (2008) 1186-1195.

[13] S.S. Mal, U. Kortz, The wheel-shaped Cu-20 tungstophosphate $Cu_{20}Cl(OH)_{24}(H_2O)_{12}(P_8W_{48}O_{184})^{25-}$ ion, Angewandte Chemie-International Edition, 44 (2005) 3777-3780.

[14] S.S. Mal, N.H. Nsouli, M.H. Dickman, U. Kortz, Organoruthenium derivative of the cyclic $H_7P_8W_{48}O_{184}^{33-}$ anion: $\{K(H_2O)\}_3\{Ru(p\text{-cymene})(H_2O)\}_4P_8W_{49}O_{186}(H_2O)_2^{27-}$, Dalton Transactions, (2007) 2627-2630.

[15] S.G. Mitchell, D. Gabb, C. Ritchie, N. Hazel, D.-L. Long, L. Cronin, Controlling nucleation of the cyclic heteropolyanion $\{P_8W_{48}\}$: a cobalt-substituted phosphotungstate chain and network, Cryst. Eng. Comm., 11 (2009) 36-39.

[16] A. Müller, M.T. Pope, A.M. Todea, H. Bogge, J. van Slageren, M. Dressel, P. Gouzerh, R. Thouvenot, B. Tsukerblat, A. Bell, Metal-oxide-based nucleation process under confined conditions: Two mixed-valence V_6-type aggregates closing the W_{48} wheel-type cluster cavities, Angewandte Chemie-International Edition, 46 (2007) 4477-4480.

[17] M. Zimmermann, N. Belai, R.J. Butcher, M.T. Pope, E.V. Chubarova, M.H. Dickman, U. Kortz, New lanthanide-containing polytungstates derived from the cyclic P_8W_{48} anion: $\{Ln_4(H_2O)_{28}[K\subset P_8W_{48}O_{184}(H_4W_4O_{12})_2Ln_2(H_2O)_{10}]^{13-}\}_x$, Ln = La, Ce, Pr, Nd, Inorganic Chemistry, 46 (2007) 1737-1740.

[18] B. Keita, Y.W. Lu, L. Nadjo, R. Contant, Salient electrochemical and electrocatalytic behaviours of the crown heteroplyanion $K_{28}Li_5H_7P_8W_{48}O_{184}\cdot 92H_2O$, Electrochemistry Communications, 2 (2000) 720-726.

[19] L.H. Bi, K. Foster, T. McCormac, E. Dempsey, Preparation of multilayer films containing a crown heteropolyanion and an osmium functionalised pyrrole monomer, Journal of Electroanalytical Chemistry, 605 (2007) 24-30.

[20] A. Sartorel, M. Carraro, G. Scorrano, B.S. Bassil, M.H. Dickman, B. Keita, L. Nadjo, U. Kortz, M. Bonchio, Iron-Substituted Polyoxotungstates as Inorganic

Synzymes: Evidence for a Biomimetic Pathway in the Catalytic Oxygenation of Catechols, Chemistry-a European Journal, 15 (2009) 7854-7858.

[21] D. Jabbour, B. Keita, L. Nadjo, U. Kortz, S.S. Mal, The wheel-shaped Cu20-tungstophosphate $[Cu_{20}Cl(H)_{24}(H_2O)_{12}(P_8W_{48}O_{184})]^{25-}$, redox and electrocatalytic properties, Electrochemistry Communications, 7 (2005) 841-847.

[22] B.S. Bassil, M. Ibrahim, S.S. Mal, A. Suchopar, R.N. Biboum, B. Keita, L. Nadjo, S. Nellutla, J. van Tol, N.S. Dalal, U. Kortz, Cobalt, Manganese, Nickel, and Vanadium Derivatives of the Cyclic 48-Tungsto-8-Phosphate $[H_7P_8W_{48}O_{184}]^{33-}$, Inorganic Chemistry, 49 (2010) 4949-4959.

[23] T. McCormac, B. Fabre, G. Bidan, Role of pH and the transition metal for the electrocatalytic reduction of nitrite with transition metal substituted Dawson type heteropolyanions .2, Journal of Electroanalytical Chemistry, 427 (1997) 155-159.

[24] S.S. Mal, M.H. Dickman, U. Kortz, A.M. Todea, A. Merca, H. Bogge, T. Glaser, A. Muller, S. Nellutla, N. Kaur, J. van Tol, N.S. Dalal, B. Keita, L. Nadjo, Nucleation process in the cavity of a 48-tungstophosphate wheel resulting in a 16-metal-centre iron oxide nanocluster, Chemistry-a European Journal, 14 (2008) 1186-1195.

[25] E.C. Constable, C.E. Housecroft, M. Cattalini, D. Phillips, Pentaerythritol-based metallodendrimers, New Journal of Chemistry, 22 (1998) 193-200.

[26] N. Anwar, M. Vagin, F. Laffir, G. Armstrong, C. Dickinson, T. McCormac, Transition metal ion-substituted polyoxometalates entrapped in polypyrrole as an electrochemical sensor for hydrogen peroxide, Analyst, 137 (2012) 624-630.

[27] N. Anwar, M. Vagin, R. Naseer, S. Imar, M. Ibrahim, S.S. Mal, U. Kortz, F. Laffir, T. McCormac, Redox Switching of Polyoxometalate-Methylene Blue based Layer-by-Layer Films, Langmuir, 28 (2012) 5480-5488.

[28] N. Fay, E. Dempsey, T. McCormac, Assembly, electrochemical characterisation and electrocatalytic ability of multilayer films based on $[Fe(bpy)^3]^{2+}$, and the Dawson heteropolyanion, $[P_2W_{18}O_{62}]^{6-}$, Journal of Electroanalytical Chemistry, 574 (2005) 359-366.

[29] M. Zynek, M. Serantoni, S. Beloshapkin, E. Dempsey, T. McCormac, Electrochemical and surface properties of multilayer films based on a Ru^{2+} metallodendrimer and the mixed addenda Dawson heteropolyanion, Electroanalysis, 19 (2007) 681-689.

[30] T. McCormac, B. Fabre, G. Bidan, Part I. A comparative electrochemical study of transition metal substituted Dawson type heteropolyanions, Journal of Electroanalytical Chemistry, 425 (1997) 49-54.

[31] A.M. Bond, T. Vu, A.G. Webb, Voltammetric studies of the interaction of the lithium cation with reduced forms of the Dawson $[S_2Mo_{18}O_{62}]^{4-}$ polyoxometalate anion, Journal of Electroanalytical Chemistry, 494 (2000) 96-104.

[32] E. Laviron, General expression of the linear potential sweep voltammogram in the case of diffusionless electrochemical systems, Journal of Electroanalytical Chemistry, 101 (1979) 19-28.

[33] C.R. Martin, I. Rubinstein, A.J. Bard, The heterogeneous rate constant for the $Ru(bpy)_3^{3+/2+}$ couple at a glassy carbon electrode in aqueous solution, Journal of Electroanalytical Chemistry, 151 (1983) 267-271.

[34] C.R. Bradbury, J. Zhao, D.J. Fermın, Distance-Independent Charge-Transfer Resistance at Gold Electrodes Modified by Thiol Monolayers and Metal Nanoparticles, Journal of Physical Chemistry C, 112 (2008) 10153–10160.

[35] M.D. Newton, J.F. Smalley, Interfacial bridge-mediated electron transfer: mechanistic analysis based on electrochemical kinetics and theoretical modelling, Physical Chemistry Chemical Physics, 9 (2007) 555-572.

[36] S. Dong, X. Xi, M. Tian, Study of the electrocatalytic reduction of nitrite with silicotungstic heteropolyanion, Journal of Electroanalytical Chemistry, 385 (1995) 227-233.

[37] D.M. Fernandes, S.M.N. Simões, H.M. Carapuça, A.M.V. Cavaleiro, Functionalisation of glassy carbon electrodes with deposited tetrabutylammonium microcrystalline salts of lacunary and metal-substituted alpha-Keggin-polyoxosilicotungstates, Electrochimica Acta, 53 (2008) 6580-6588.

[38] J.E. Toth, F.C. Anson, Electrochemical properties of iron(III)-substituted heteropolytungstate, Journal of Electroanalytical Chemistry, 256 (1988) 361-370.

[39] M. Ammam, B. Keita, L. Nadjo, J. Fransaer, Nitrite sensor based on multilayer film of Dawson-type tungstophosphate $K_7[H_4PW_{18}O_{62}]\cdot 18H_2O$ immobilized on glassy carbon, Talanta, 80 (2010) 2132-2140.

[40] L. Cheng, J.A. Cox, Preparation of multilayered nanocomposites of polyoxometalates and poly(amidoamine) dendrimers, Electrochemistry Communications, 3 (2001) 285-289.

[41] D.M. Fernandes, H.M. Carapuca, C.M.A. Brett, A.M.V. Cavaleiro, Electrochemical behaviour of self-assembly multilayer films based on iron-substituted alpha-Keggin polyoxotungstates, Thin Solid Films, 518 (2010) 5881-5888.

[42] S. Imar, C. Maccato, C. Dickinson, F. Laffir, M. Vagin, T. McCormac, Enhancement of Nitrite and Nitrate Electrocatalytic Reduction through the Employment of Self-Assembled Layers of Nickel and Copper-Substituted Crown-Type Heteropolyanions, Langmuir, 31 (2015) 2584-2592.

[43] L. Liu, L. Tian, H. Xu, N. Lu, Electrochemical properties of organo-titanium substituted heteropolytungstate and its electrocatalytic reduction of nitrite, Journal of Electroanalytical Chemistry, 587 (2006) 213-219.

[44] R. Naseer, S.S. Mal, M. Ibrahim, U. Kortz, G. Armstrong, F. Laffir, C. Dickinson, M. Vagin, T. McCormac, Redox, surface and electrocatalytic properties of layer-by-layer films based upon Fe(III)-substituted crown polyoxometalate $[P_8W_{48}O_{184}Fe_{16}(OH)_{28}(H_2O)_4]^{20-}$, Electrochimica Acta, 134 (2014) 450-458.

[45] J. Zhang, J.K. Goh, W.T. Tan, A.M. Bond, Mechanistic analysis of the electrocatalytic properties of dissolved alpha and beta isomers of $[SiW_{12}O_{40}]^{4-}$ and solid $[Ru(bipy)_3]_2[\alpha\text{-}SiW_{12}O_{40}]$ on the reduction of nitrite in acidic aqueous media, Inorganic Chemistry, 45 (2006) 3732-3740.

[46] M. Zhou, L.P. Guo, F.Y. Lin, H.X. Liu, Electrochemistry and electrocatalysis of polyoxometalate-ordered mesoporous carbon modified, Analytica Chimica Acta, 587 (2007) 124-131.

[47] J.F. Moulder, W.F. Stickle, P.E. Sobol, K.D. Bomben, Handbook of X-Ray Photoelectron Spectroscopy: a reference book of standard spectra for identification and interpretation of XPS data, Perkin-Elmer Corporation, Physical Electronics Division, Minneapolis, USA, 1992.

[48] NIST-XPS database, version 3.5.

[49] B. Xu, L. Xu, G. Gao, Y. Jin, Nanosized multilayer films with concurrent photochromism and electrochromism based on Dawson-type polyoxometalate, Applied Surface Science, 253 (2007) 3190-3195.

Figure legends

Figure 1. Electrochemical properties of crown-type POM multi-substituted by transition metal ions in solution. **A:** Effect of pH on the voltammetric responses. Cyclic voltammograms have been recorded at GCE in 0.5 M H_2SO_4 (solid line) and in pH 4.5 buffer (dashed lines) solution (1 mM) of Co_6POM (scan rate 10 mV s^{-1}). **B-F:** Effect of substitution by transition metal ion of POM on the electrocatalytic capabilities for nitrite reduction in solution. Cyclic voltammograms have been recorded at GCE in 1 mM solutions of precursor (**B**), Fe_{16}POM (**C**), Co_6POM (**D**) and Ni_7POM (**E**) before and after additions (dashed lines) of 2 mM solution of sodium nitrite (pH 4.5 buffer, scan rate 10 mV s^{-1}). **F:** Calibrations plots of electrocatalytic reduction of sodium nitrite by Fe_{16}POM (▲), Ni_7POM (△), Co_6POM (○) and their precursor (■).

Figure 2. Assembly of Co_6POM-RuD LBL-films monitored by voltammetry. Consecutive cyclic voltammograms obtained at GCE electrode modified with of LBL films with POM terminal layers (**A**) and with RuD terminal layers (**B**). **C**: the dependences of peak charges of $Ru^{II/III}$ redox process on the number of layers (□ and ■ – charges of cathodic and anodic peaks correspondingly). Scan rate 10 mV s^{-1}, pH 2.

Figure 3. Assembly of Co_6POM-RuD LBL-films monitored by impedance spectroscopy. **A**: Nyquist plot of impedance spectra recorded at LBL film-modified electrode at solution of redox probe (10 mM $K_3[Fe(CN)_6]$, 10 mM $K_4[Fe(CN)_6]$, 0.1M KCl); solid lines – fitting curves. 1 - spectrum of blanck electrode; 2 - spectrum of PDDA-modified electrode; 3, 5 and 7 - spectra of modified electrode after first and third and fifth assembly steps (POM as terminal layer); 4, 6 and 8 - spectra of modified electrode after second, forth and sixth assembly step (RuD as terminal layer). 5 mV amplitude, 230 mV potential of measurement. Inset: high frequency plot. **B**: dependence of fitted values of charge transfer resistance on the assembly number of LBL films based on Ni_7POM (○) and Co_6POM (■).

Figure 4. Porosity of Co_6POM-RuD LBL-films towards $[Ru(NH_3)_6]^{3+/2+}$ redox probe diffusion. Cyclic voltammograms were recorded at pH 2 buffer before (thin line) and

after (thick line) addition of 1 mM $[Ru(NH_3)_6]Cl_3$. Dashed line – voltammogram of redox probe at blank GCE. **A**: electrode modified with LBL film of 8 assembly steps (POM as a terminal layer); **B**: film of 9 assembly steps with RuD terminal layer; **C**: film of 16 assembly steps (POM as a terminal layer); **D**: film of 17 steps (RuD as a terminal layer). Scan rate 10 mV s^{-1}, pH 2.

Figure 5. Calibration plot of nitrite electrocatalytic reduction at the electrode modified by Ni_7POM-RuD LBL film of 16 assembly steps. Inset: cyclic voltammograms obtained in absence (solid line) and after additions of sodium nitrite (dashed lines): 0.5, 1, 1.5, and 2 mM. Scan rate 5 mV s^{-1}, pH 4.5.

Figure 6. Evolution of topography observed during the LBL film assembly. The AFM images obtained for bare ITO (**A**) and for slides modified by Ni_7POM LBL film with POM (**B**) and RuD (**C**) as a terminal layers (14 and 15 assembly steps, respectively); **D**: SEM micrograph of Co_6POM-RuD LBL film (12 assembly steps); **E**: the dependences of the root mean square height of the surface on the assembly number assessed from AFM data for LBL films based on Ni_7POM (■) and Co_6POM (○).

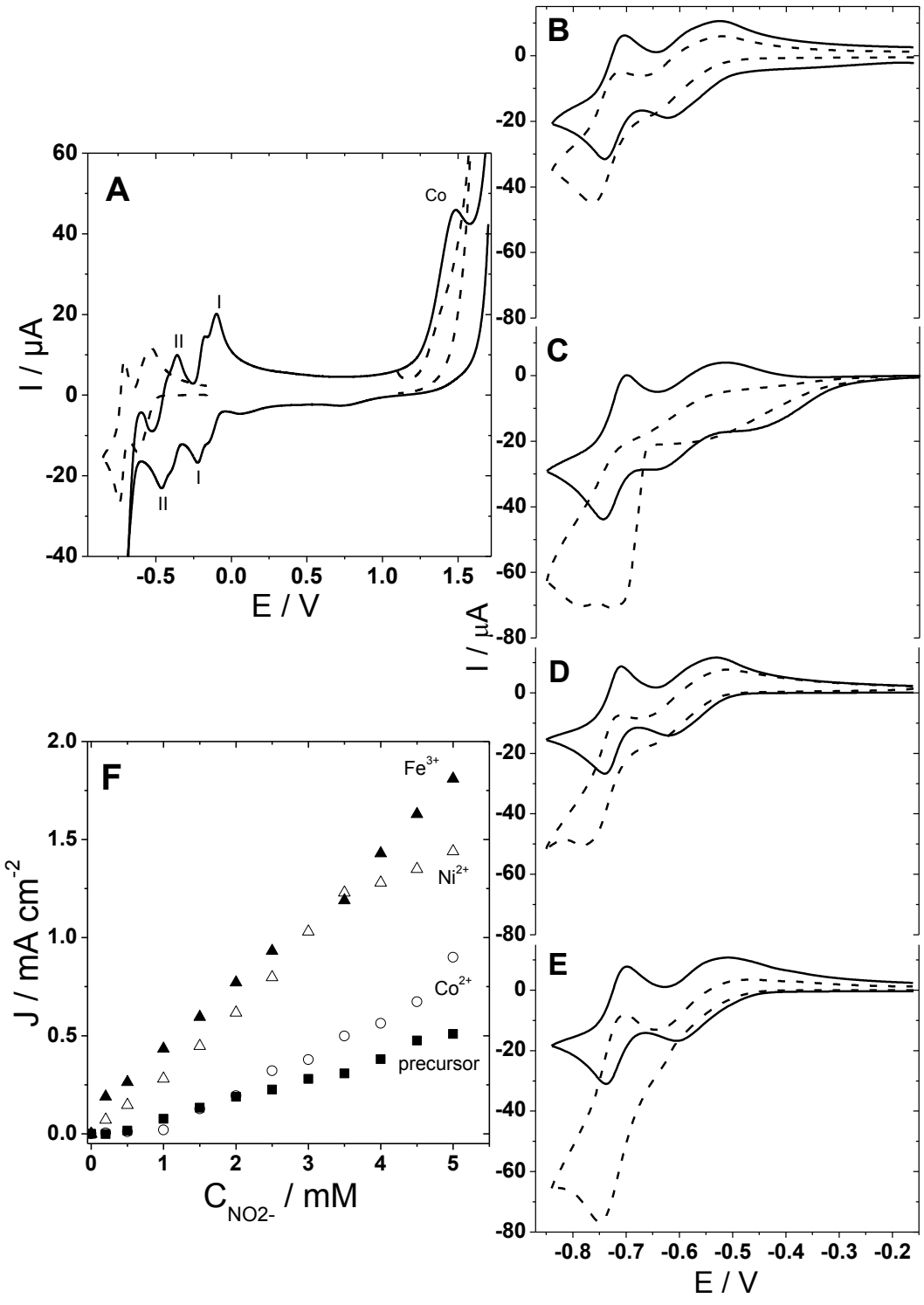
A
Co
I
II
I
II
I / µA
E / V
B
C
D
E
I / µA
E / V
F
Fe3+
Ni2+
Co2+
precursor
J / mA cm-2
C NO2- / mM

Figure 1.

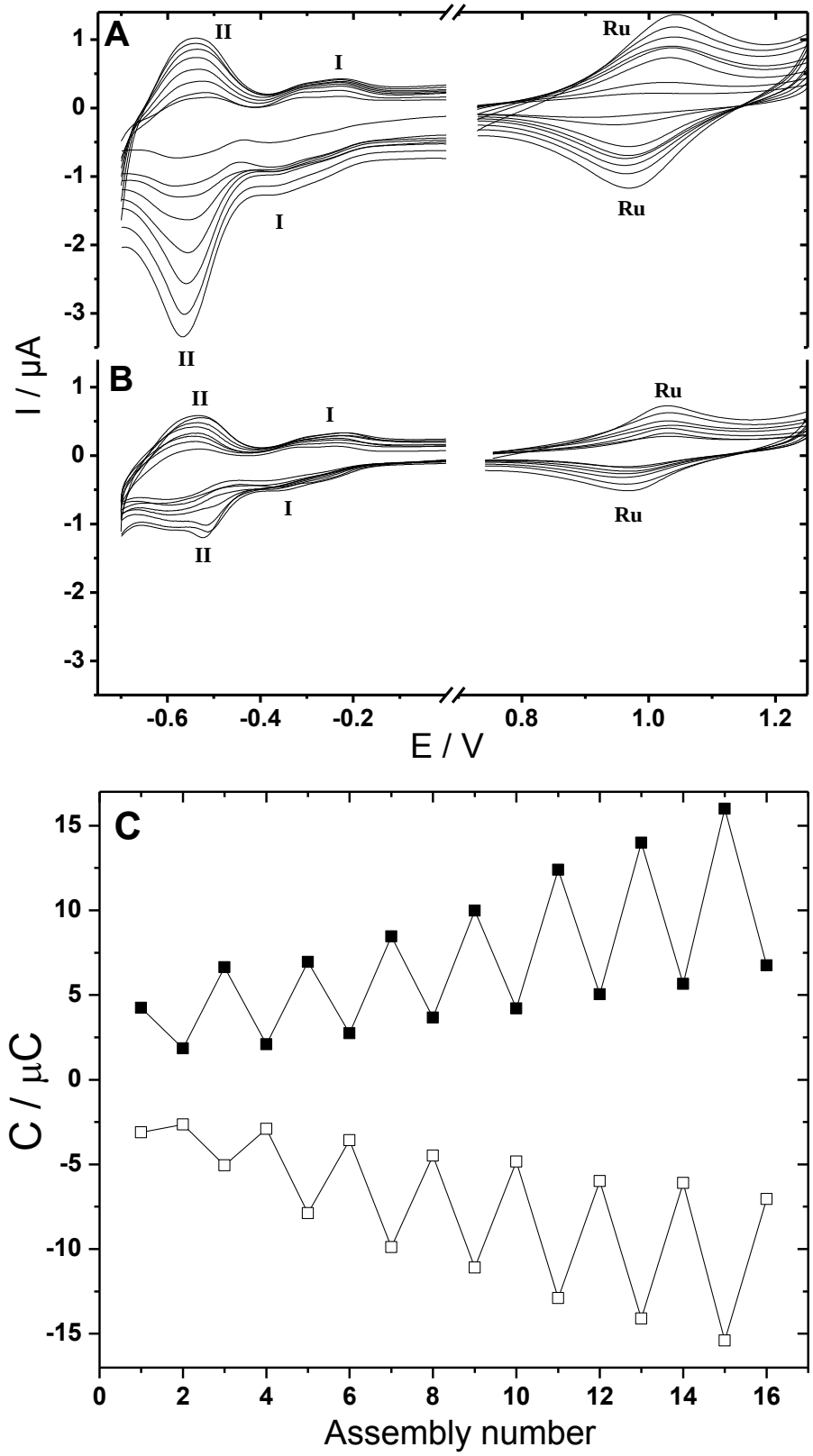

Figure 2.

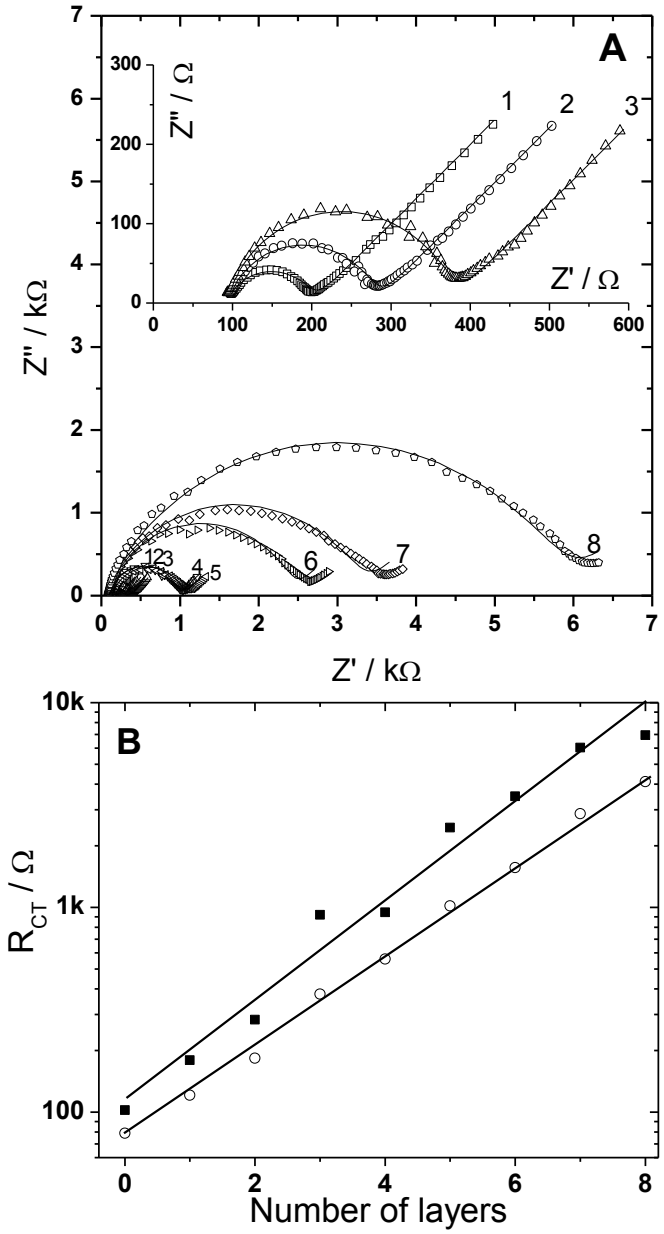

Figure 3.

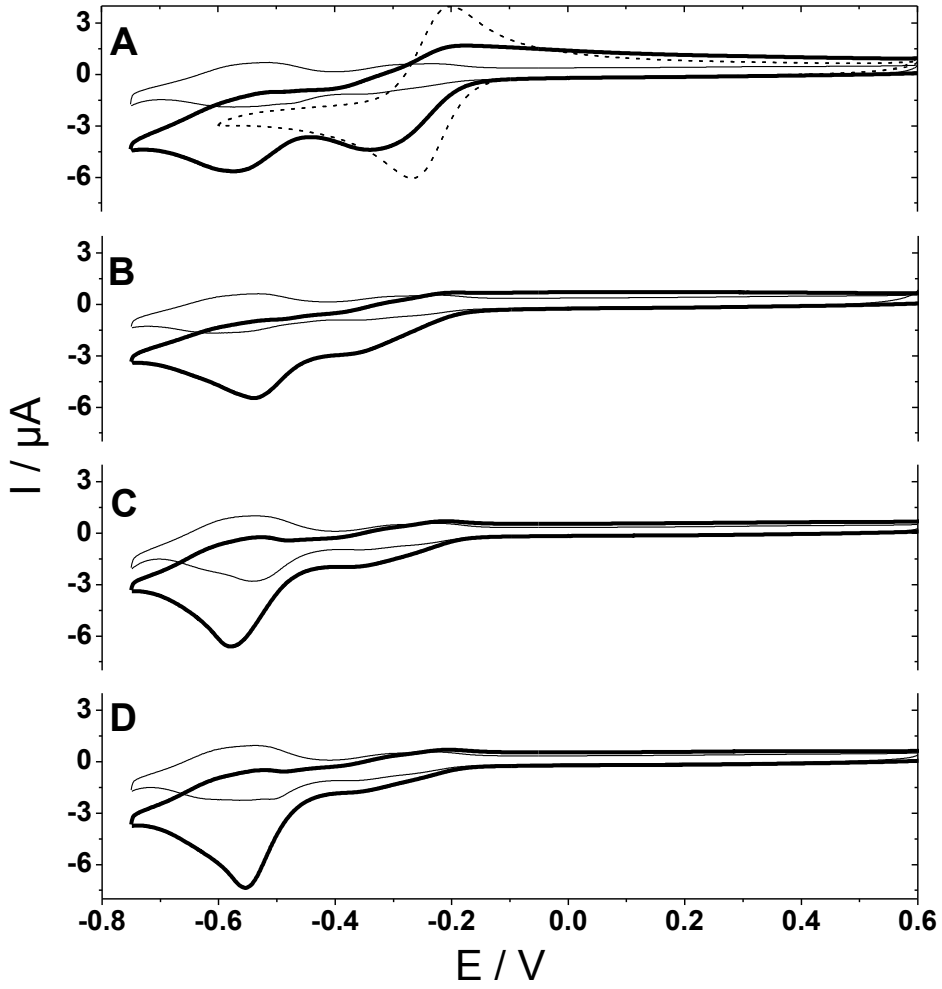

Figure 4.

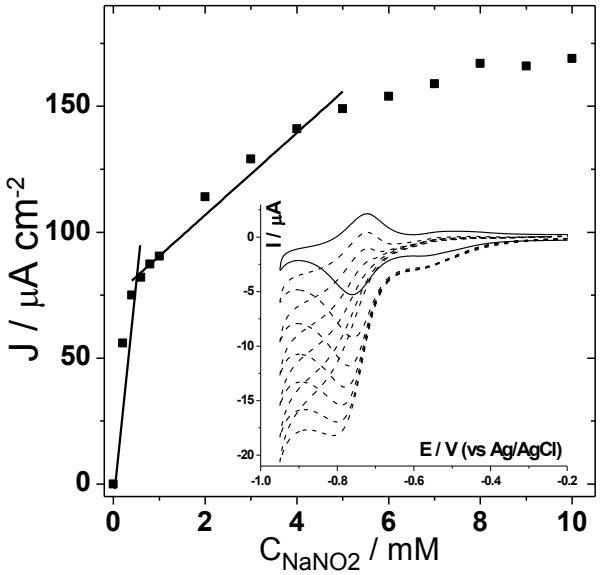
J / μA cm-2
150
100
50
0
0
2
4
6
8
10
C NaNO2 / mM
I / μA
0
-5
-10
-15
-20
-1.0
-0.8
-0.6
-0.4
-0.2
E / V (vs Ag/AgCl)

Figure 5.

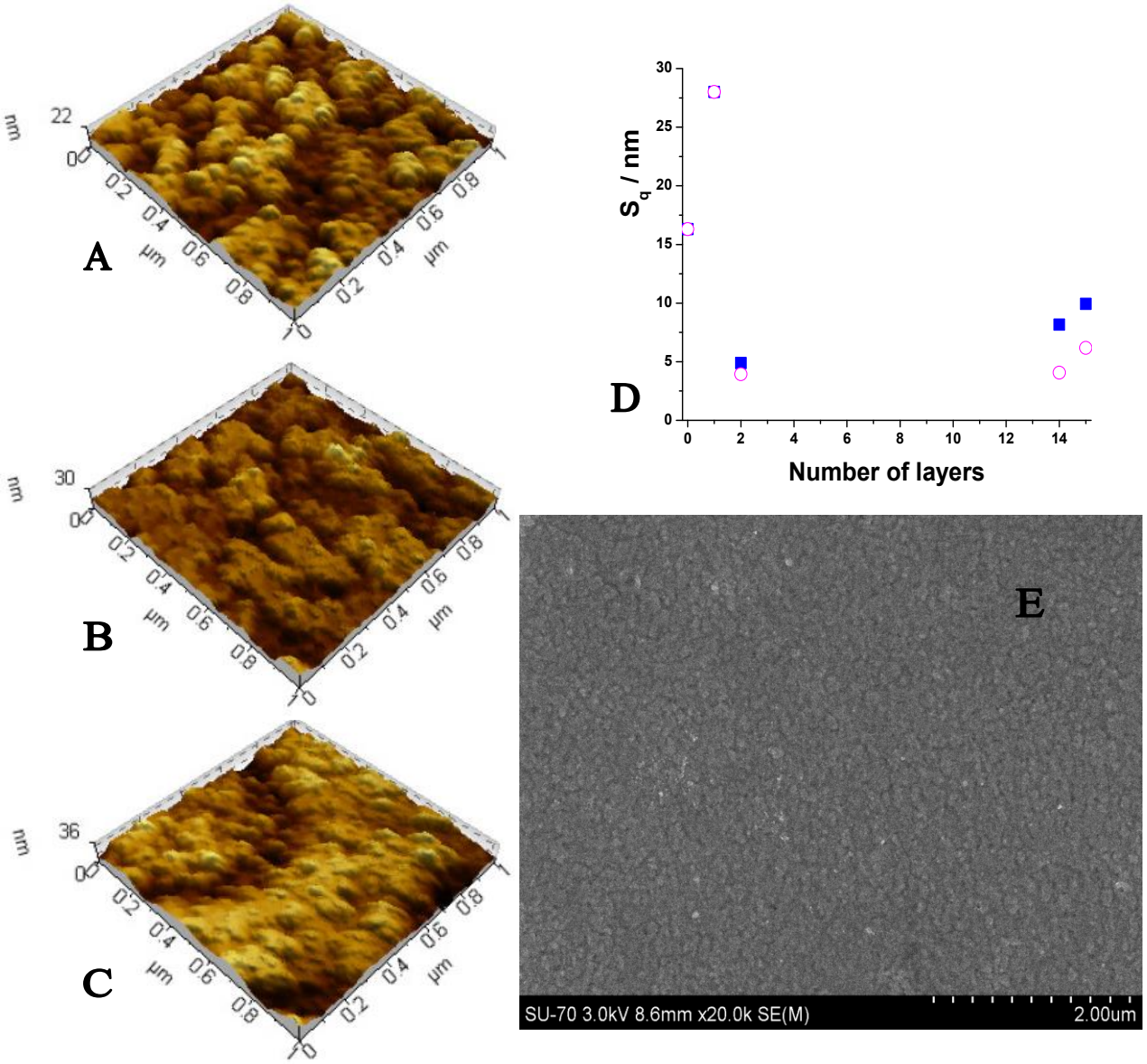
A
B
C
D
E
nm
22
30
36
μm
S_q / nm
Number of layers
SU-70 3.0kV 8.6mm x20.0k SE(M)
2.00um

Figure 6.

SUPPORTING INFORMATION

Electrocatalysis by crown-type polyoxometalates multi-substituted by transition metal ions; Comparative study

Rashda Naseer,[a] Sib Sankar Mal,[b,x] Ulrich Kortz,[b] Gordon Armstrong,[c] Fathima Laffir,[c] Calum Dickinson,[c] Mikhail Vagin*,[d] Timothy McCormac[a]

[a]Electrochemistry Research Group, Department of Applied Science, Dundalk Institute of Technology, Dublin Road Dundalk, County Louth, Ireland

[b]Jacobs University, Department of Life Sciences and Chemistry, P.O. Box 750561, 28725 Bremen, Germany

[c]Materials and Surface Science Institute, University of Limerick, Limerick, Ireland

[d]Department of Physics, Chemistry and Biology, Linköping University, SE-581 83, Linköping, Sweden; tel.: +46702753087; mikva@ifm.liu.se

[x]Current address: Department of Chemistry, Science Block, NITK Surathkal, Mangalore-575025, India

*Corresponding author

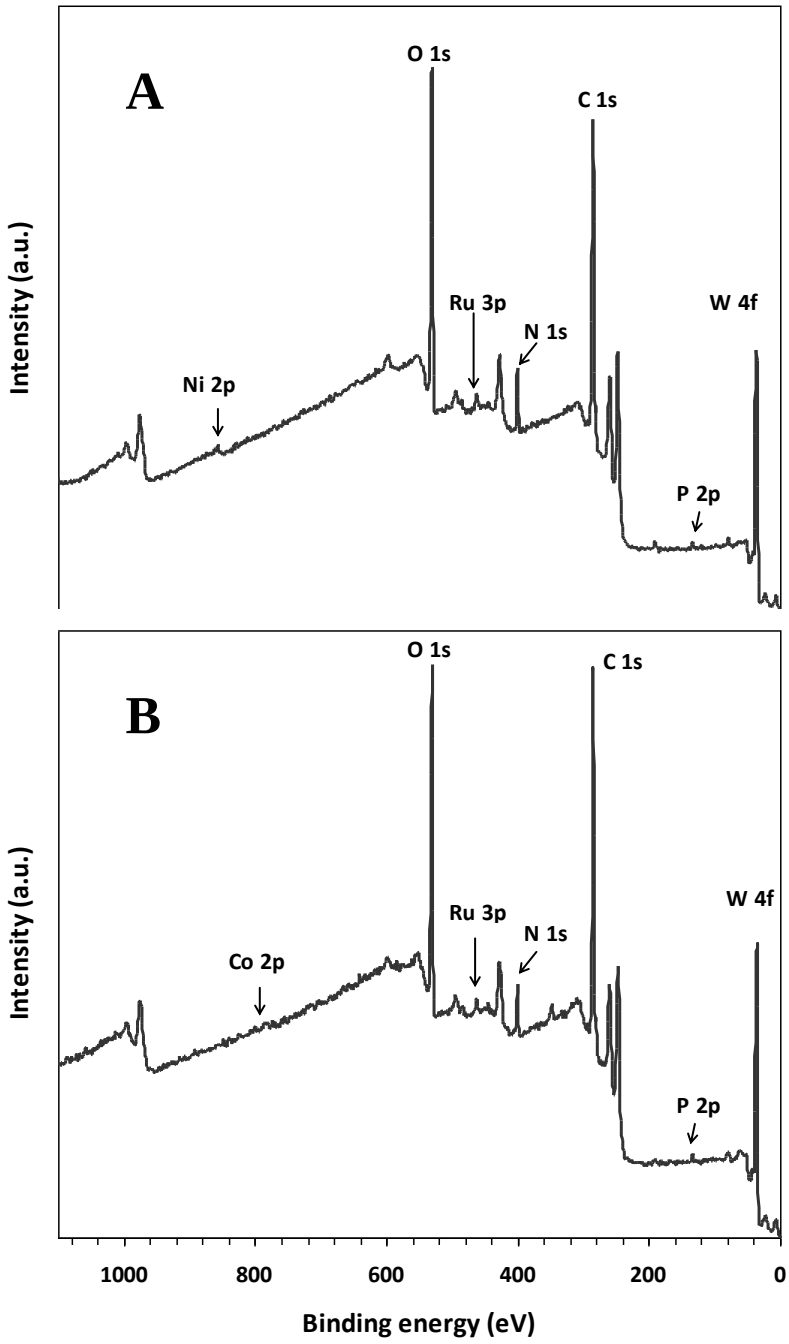

Figure S1. Survey spectra of LBL films based on Ni_7POM (**A**) and Co_6POM (**B**).

Table S1. Relative composition of LBL films analysed by XPS

Atomic %

$P_8W_{48}O_{184}$	**Ni**	**Co**	**O**	**N**	**C**	**P**	**W**	**Ru**	**K**
Ni^{2+}-substituted	0.4	-	29.2	6.2	56.3	1.1	5.6	0.9	0.5
Co^{2+}-substituted	-	0.4	28.7	5.7	56.8	1.3	5.8	0.9	